Available online at www.sciencedirect.com
ScienceDirect
Trans. Nonferrous Met. Soc. China 22(2012) 2421−2430
Transactions of Nonferrous Metals Society of China
www.tnmsc.cn

FEM simulation and experimental verification of temperature field and phase transformation in deep cryogenic treatment

LI Jun-wan[1], TANG Lei-lei[1], LI Shao-hong[2], WU Xiao-chun[1]

1. School of Materials Science and Engineering, Shanghai University, Shanghai 200072, China;
2. School of Materials Science and Engineering, Kunming University of Science and Technology, Kunming 650093, China

Received 9 July 2012; accepted 3 August 2012

Abstract: Combining with the low temperature material properties and the boiling heat transfer coefficient of specimen immersed in the liquid nitrogen, a numerical model based on metallo-thermo-mechanical couple theory was established to reproduce the deep cryogenic treatment (DCT) process of a newly developed cold work die steel Cr8Mo2SiV (SDC99). Moreover, an experimental setup for rapid temperature measurement was designed to validate the simulation results. The investigation suggests that the differences in temperature and cooling rate between the surface and core of specimen are very significant. However, it should be emphasized that the acute temperature and cooling rate changes during DCT are mainly concentrated on the specimen surface region about 1/3 of the sample thickness. Subjected to DCT, the retained austenite of quenched specimen continues to transform to martensite and finally its phase volume fraction reduces to 2.3%. The predicted results are coincident well with the experimental data, which demonstrates that the numerical model employed in this study can accurately capture the variation characteristics of temperature and microstructure fields during DCT and provide a theoretical guidance for making the reasonable DCT procedure.
Key words: deep cryogenic treatment; boiling heat transfer coefficient; finite element method; phase transformation; cold work tool steel

1 Introduction

Deep cryogenic treatment (DCT) is an additive process to the conventional heat treatment of cold work tool steel and usually involves cooling to liquid nitrogen temperature around −196 °C [1]. This technique has been proven to be efficient in improving the physical and mechanical properties of the various materials such as wear, abrasion, erosion/corrosion resistivity, durability and stability [2,3]. However, DCT is a complex process involving thermal, metallurgical and mechanical phenomena. It is still difficult, even impossible to investigate in situ all these physical phenomena correctly and efficiently with the current experimental test systems.

Recently, some mathematical models describing the coupled interactions among the temperature field, the microstructure field and the stress−strain field during the quenching are built to provide a theoretical guidance to the heat treatment [4,5]. Aside from the mathematical models, to perform the simulation of DCT process, there are two extremely important characteristics of material that must be obtained. 1) The low temperature material properties. Due to the limitations of the test conditions, there is a serious lack of the low temperature physical and mechanical properties of material and the existing ones also lack sufficient accuracy to meet the requirements of simulation. 2) The boiling heat transfer coefficient between the specimen surface and the liquid nitrogen. It is very difficult to accurately measure the boiling heat transfer coefficient by experimental methods. Due to these factors, the numerical simulation of DCT has not yet received widespread attention. So far, most of the available researches [6−8] are still limited to estimate the temperature field evolution during DCT and neglect the phase transformation and its latent heat effects.

The main objective of this work is to reproduce the DCT process considering phase transformation and its latent heat effects using finite element method (FEM), and to explore the temperature and microstructure distribution rules of specimen immersed in the liquid

Foundation item: Project (51171104) supported by the National Natural Science Foundation of China
Corresponding author: LI Jun-wan; Tel: +86-21-56331153; Fax: +86-21-56331461; E-mail: lijunwan@shu.edu.cn
DOI: 10.1016/S1003-6326(11)61480-5

nitrogen so as to provide a theoretical guidance for making the more efficient and reasonable DCT procedure.

2 Mathematical formulation

2.1 Determination of temperature distribution

According to Fourier law, the transient heat conduction with the latent heat of phase transformation during DCT can be written as [5,9]:

$$\rho c\frac{\partial T}{\partial t}=\frac{\partial}{\partial x}(\lambda\frac{\partial T}{\partial x})+\frac{\partial}{\partial y}(\lambda\frac{\partial T}{\partial y})+\frac{\partial}{\partial z}(\lambda\frac{\partial T}{\partial z})+Q \tag{1}$$

where ρ, c and λ are the density, specific heat capacity and thermal conductivity of the material given as a function of temperature T, respectively; t is time and Q is the latent heat due to phase transformation.

The initial condition at time t=0 can be expressed as:

$$T|_{t=0}=T_0(x,y,z) \tag{2}$$

where $T_0(x, y, z)$ is the initial temperature function. The boundary condition of quenching belongs to the third type condition and can be described as:

$$-\lambda\left.\frac{\partial T}{\partial n}\right|_{\Gamma}=H(T_{\mathrm{B}}-T_{\mathrm{E}}) \tag{3}$$

where n is the outer normal boundary of surface; T_{B} and T_{E} are the temperatures of boundary and environment, respectively; H is the heat transfer coefficient, which will be acquired by an empirical formula method in this study and the detail will be discussed in the following section.

In this study, the latent heat of phase transformation is regarded as the internal heat source [9], which is a function of phase transformation rate and temperature:

$$Q=\Delta H\frac{\xi_{n+1}-\xi_n}{t_{n+1}-t_n}=\Delta H\Delta\xi \tag{4}$$

where t_{n+1} and t_n are the times of (n+1)th and nth simulation steps; ξ_{n+1} and ξ_n are the phase transformation volume fractions corresponding to t_{n+1} and t_n, respectively; $\Delta\xi$ is the phase transformation volume fraction of unit time and ΔH is the enthalpy of austenite transformation, which is summarized in Table 1 [10].

Table 1 Enthalpy (ΔH) of austenite phase transformation (J/m^3)

Ferrite (F)	Pearlite (P)	Bainite (B)	Martensite (M)
5.9×10^8	6.0×10^8	6.2×10^8	6.5×10^8

2.2 Determination of microstructure distribution

Phase transformations that occur during the cooling process in quenching can be classified into the diffusion-controlled and non-diffusion-controlled ones. For the diffusion-controlled phase transformation, the Johnson-Mehl-Avrami (JMA) kinetic model is applied for evaluating volume fractions of ferrite (F), pearlite (P) and bainite (B). Using this isothermal kinetic model, the transformed fraction can be predicted as a function of time [11]:

$$\xi=1-\exp(-bt^n) \tag{5}$$

$$n=\frac{\ln\left[\ln(1-\xi_1)/\ln(1-\xi_2)\right]}{\ln(t_1/t_2)} \tag{6}$$

$$b=-\frac{\ln(1-\xi_1)}{t_1^n} \tag{7}$$

where b and n are the material kinetic parameters; t_1 and t_2 are the isothermal times at certain temperature; ξ_1 and ξ_2 are the volume fractions of phase transformations corresponding to t_1 and t_2, respectively. All parameters for this calculation dependent on TTT diagram are taken from the start volume fraction 1% and end volume fraction 99% of TTT curves in logarithmic function of transformation time, which is a function of temperature, stress and carbon content.

For the non-diffusion-controlled phase transformation, the transformed fraction of martensite is calculated as a function of temperature using the modified rule by INOUE et al [12]:

$$\xi=1-\exp(\psi_1T+\psi_2(C-C_0)+\psi_{31}\sigma_{\mathrm{m}}+\psi_{32}\bar{\sigma}+\psi_4) \tag{8}$$

where σ_{m} and $\bar{\sigma}$ are the mean and effective stresses, respectively; C is the carbon content; ψ_1, ψ_2, ψ_3 and ψ_4 are coefficients which can be attained by calculation in TTT curve. When the martensitic transformation start temperatures (M_{s}) under carburized conditions and applied stress are given, ψ_2/ψ_1, ψ_{31}/ψ_1 and ψ_{32}/ψ_1 can be determined. If the temperatures for martensitic transformation start (M_{s}) and for 99% martensite at ξ=0 and ξ=0.99 are provided respectively, ψ_1 and ψ_4 can be identified.

2.3 Determination of stress and strain field

The prediction of stress and strain is based on the plastic flow stress within the isotropic thermo-elasto-plastic material behavior of an individual phase of austenitic (A), ferrite (F), pearlite (P), bainite (B) and martensite (M). Because the plastic distortion generated in the heat treatment process is so small that the following flow stress model is accurate enough [13].

$$\bar{\sigma}=Y(T,C)+H(T,C)\bar{\varepsilon} \tag{9}$$

where $\bar{\sigma}$ is the flow stress; Y and H are the yield strength and strain hardening modulus, respectively, which are functions of temperature and carbon content; $\bar{\varepsilon}$ is the effective plastic strain. The total strain rate is assumed as the sum of individual strain rate caused by different physical sources as:

$$\dot{\varepsilon}_{ij} = \dot{\varepsilon}_{ij}^{\mathrm{e}} + \dot{\varepsilon}_{ij}^{\mathrm{p}} + \dot{\varepsilon}_{ij}^{\mathrm{th}} + \dot{\varepsilon}_{ij}^{\mathrm{pt}} + \dot{\varepsilon}_{ij}^{\mathrm{tp}} \quad (10)$$

where $\dot{\varepsilon}_{ij}$, $\dot{\varepsilon}_{ij}^{\mathrm{e}}$, $\dot{\varepsilon}_{ij}^{\mathrm{p}}$, $\dot{\varepsilon}_{ij}^{\mathrm{th}}$, $\dot{\varepsilon}_{ij}^{\mathrm{pt}}$ and $\dot{\varepsilon}_{ij}^{\mathrm{tp}}$ denote total, elastic, plastic, thermal, dilatational phase transformation and transformation plasticity, respectively.

3 Boiling heat transfer model

The boiling heat transfer coefficient between the specimen surface and the liquid nitrogen is a key parameter for DCT analysis. Recently, many methods such as empirical formula method, lumped heat capacity method, fixed heat flux method and inverse heat transfer method [14−16], have been widely adopted to obtain the boiling heat transfer coefficient. In particular, the empirical formula method has become a relatively common method owing to its simplicity. According to the classical boiling theory, the boiling curve can be divided into four stages: natural convection, nucleate boiling, transition boiling and stable film boiling [17].

For the natural convection heat transfer, it can be described by [15]:

$$\frac{c_{\mathrm{LN}}\Delta T}{i_{\mathrm{fg}}} < 5\times10^{-5}\cdot(Gr_{\mathrm{b}})^{0.2}\cdot(Pr_{\mathrm{LN}})^{2.66} \quad (11)$$

where ΔT is the temperature difference between the specimen surface and the saturated liquid nitrogen, c_{LN} and i_{fg} are the specific heat capacity at constant pressure and the latent heat of vaporization of saturated liquid nitrogen, respectively, Pr_{LN} and Gr_{b} are Prandtl number and Grashof number.

For the nucleate boiling heat transfer, it can be determined based on ROHSENOW's equation [18]:

$$\frac{c_{\mathrm{LN}}\Delta T}{i_{\mathrm{fg}}(Pr_{\mathrm{LN}})^{n}} = C_{\mathrm{sf}}\left[\frac{q}{\mu_{\mathrm{LN}} i_{\mathrm{fg}}}\sqrt{\frac{g_{\mathrm{c}}\sigma_{\mathrm{LN}}}{g(\rho_{\mathrm{LN}}-\rho_{\mathrm{G}})}}\right]^{1/3} \quad (12)$$

where n is an empirical index, which is assumed as 1.7 for the liquid nitrogen; C_{sf} is the roughness coefficient of fluid/material combination; q is the heat flux; μ_{LN}, ρ_{LN} and σ_{LN} are the dynamic viscosity, density and surface tension of liquid nitrogen, respectively; ρ_{G} is the density of nitrogen; g and g_{c} are the gravity acceleration and the ratio of the gravity acceleration to the microgravity acceleration.

For the transition boiling heat transfer, so far there is no accepted empirical formula available. Therefore, in this study, a general linearized polynomial interpolation is used to calculate the boiling heat transfer coefficient. Meanwhile, the test results are used to verify the validity of the interpolation scheme.

For the stable film boiling heat transfer, when the vapour film is in a state of laminar flow, it can be described by ELLION's laminar film boiling equation [15,19]:

$$Nu = 0.714(Ra_{\mathrm{b}}/Ja_{\mathrm{G}})^{1/4} \quad (13)$$

When the vapour film is in a state of turbulent flow, it can be expressed by HSU and WESTWATER's turbulent film boiling equation [15,19]:

$$Nu = 0.2(Ra_{\mathrm{b}})^{2/5}(Ja_{\mathrm{G}})^{1/5}(Pr_{\mathrm{G}})^{3/5} \quad (14)$$

where Nu is the Nusselt number; Ja_{G} and Pr_{G} are Jacob number and Prandtl number at constant pressure of nitrogen.

According to WESTWATER's boiling test results, when different types of metals are immersed in the liquid nitrogen bath, the critical heat flux (CHF) and its temperature difference have the following forms [14]:

$$\frac{q_{\mathrm{CHF,A}}}{q_{\mathrm{CHF,B}}} = \left[\frac{(k\rho c)_{\mathrm{A}}}{(k\rho c)_{\mathrm{B}}}\right]^{0.18} \quad (15)$$

$$\frac{\Delta T_{\mathrm{CHF,A}}}{\Delta T_{\mathrm{CHF,B}}} = \left[\frac{(k\rho c)_{\mathrm{A}}}{(k\rho c)_{\mathrm{B}}}\right]^{-0.23} \quad (16)$$

$$\frac{\Delta T_{\mathrm{Min,A}}}{\Delta T_{\mathrm{Min,B}}} = \left[\frac{(k\rho c)_{\mathrm{A}}}{(k\rho c)_{\mathrm{B}}}\right]^{-0.18} \quad (17)$$

where $q_{\mathrm{CHF,A}}$, $\Delta T_{\mathrm{CHF,A}}$ and $q_{\mathrm{CHF,\,B}}$, $\Delta T_{\mathrm{CHF,\,B}}$ are the critical heat flux and temperature difference of metals A and B corresponding to the nucleate boiling heat transfer stage, respectively; $\Delta T_{\mathrm{Min,A}}$ and $\Delta T_{\mathrm{Min,B}}$ are the minimum temperature difference of metals A and B corresponding to the film boiling heat transfer stage; $(k\rho c)_{\mathrm{A}}$ and $(k\rho c)_{\mathrm{B}}$ are the thermal diffusivity of metals A and B. Combined with the above empirical mathematical models and the literatures, the boiling heat transfer coefficient of steel part immersed in the liquid nitrogen bath can be determined, as presented in Fig. 1.

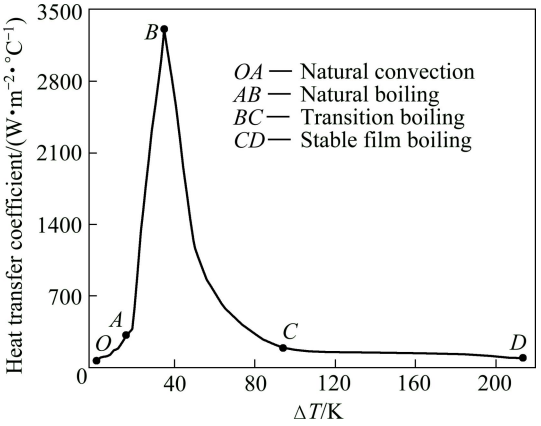

Fig. 1 Boiling heat transfer coefficient of SDC99 specimen in liquid nitrogen bath

4 Experimental

4.1 Test specimen

A commercial newly developed cold work die steel Cr8Mo2SiV (SDC99) was used to prepare specimens in this investigation. The chemical composition is given in Table 2. The specimen has the size of 60 mm in length, 60 mm in width and 100 mm in thickness. In order to acquire the thermal history during DCT, four 5 mm-diameter holes were designed in different positions of the specimen to install the sheathed PT100 thermocouple, as shown in Fig. 2. After DCT, the contents of retained austenite and martensite were measured with X-ray diffraction instrument (DLMax-2550, Rigaku, Japan) with Cu K_α (λ=1.5418×10^{-10} m) X-ray source. The volume fraction of retained austenite and martensite before and after DCT are approximately 20.3% and 79.7%, 2.8% and 97.2%, respectively.

Table 2 Chemical composition of cold work die steel SDC99 (mass fraction, %)

C	Si	Mn	Cr	Mo
0.91	0.51	0.30	8.86	1.47
V	P	S	Fe	
0.3	0.01	0.0008	Bal.	

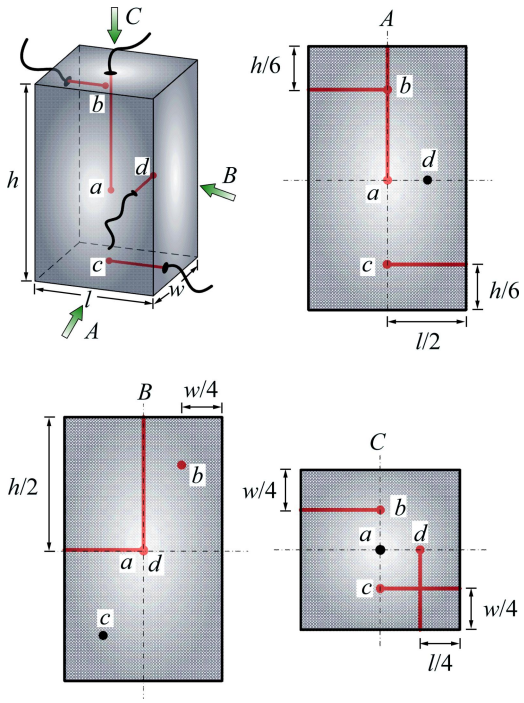

Fig. 2 Specimen geometry and temperature measurement positions

4.2 Low temperature material properties

The measurements of low temperature thermal conductivity and specific heat capacity were performed in physical property measurement system (PPMS, Quantum Design, Inc., USA). The elastic modulus was measured by the free resonance method using an elastic modulus and internal friction meter (EG-series, Nihon Techno-Plus Co., Ltd, Japan). The low temperature thermal conductivity and specific heat capacity of the cold work die steel SDC99 as well as the elastic modulus as functions of temperature are given in Fig. 3.

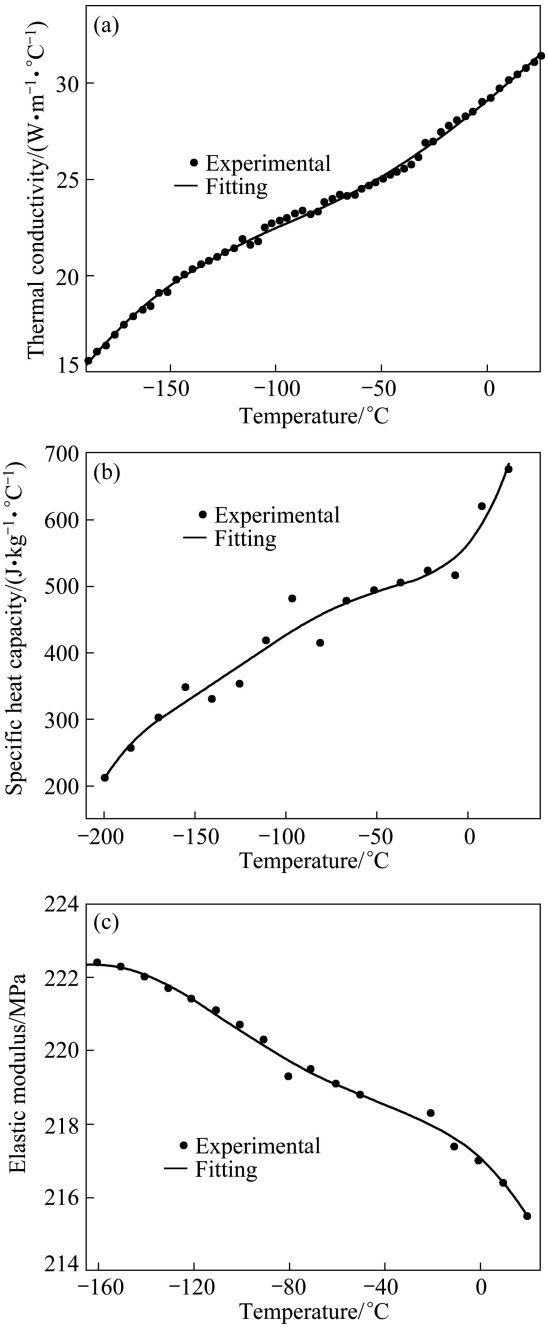

Fig. 3 Low temperature material properties of SDC99: (a) Thermal conductivity; (b) Specific heat capacity; (c) Elastic modulus

4.3 Time temperature transformation (TTT) diagram

In order to determine the kinetic parameters for phase transformation kinetic models, it is very important

to correctly acquire the dilatometric properties of SDC99 during continuous cooling and its time−temperature−transformation (TTT) diagram. The dilatometer (DIL-805L, BÄHR-Thermoanalyse GmbH, Germany) was used to measure the transformation strains during austenite decomposition under the continuous cooling conditions. By combining the dilatometric test with the calculation of equilibrium solidification behaviour using JMatPro® software [20], the time−temperature−transformation (TTT) diagram can also be obtained, as shown in Fig. 4.

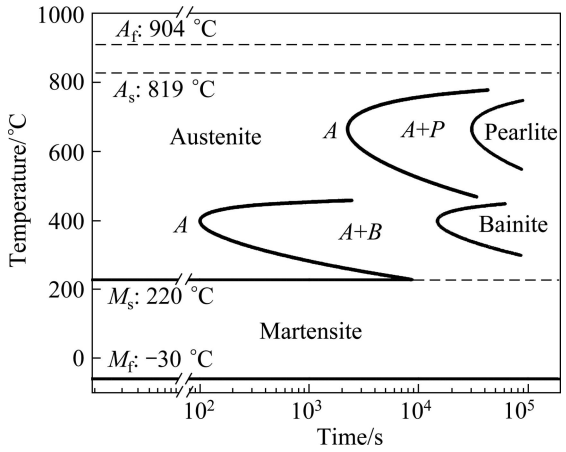

Fig. 4 Time−temperature−transformation (TTT) diagram of SDC99 obtained by dilatometric test and thermodynamic calculation using JMatPro® software

4.4 Deep cryogenic treatment (DCT)

Figure 5 shows a schematic diagram illustrating the DCT process used in this study. The experimental setup used for temperature history test during DCT includes SDC99 specimen, liquid nitrogen, thermocouple (Pt100), multi-channel data logger (GL820, GARPHTEC Co., Ltd, Japan), dewar and supporting shelf. During DCT, the temperature data of SDC99 specimen were automatically collected by means of multi-channel data logger with an interval of 1 s. After DCT, the specimen was put in air to recover at room temperature. The measurement was repeated three times for accuracy and the average data were presented.

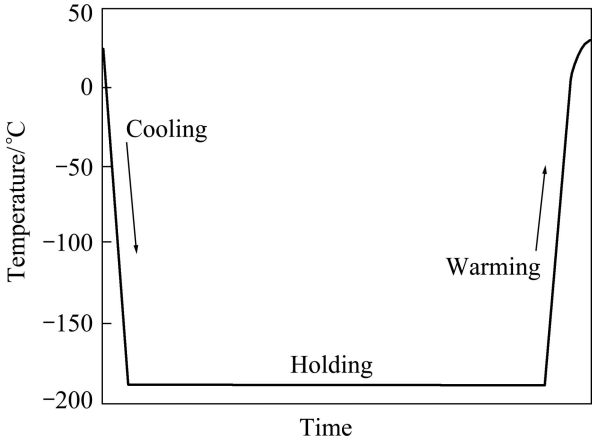

Fig. 5 Schematic diagram of DCT process

5 Numerical procedure

The geometry and three-dimensional FEM model of specimen prepared for DCT simulation are illustrated in Fig. 6. The total numbers of nodes and elements are 70434 and 14143, respectively. Moreover, to further discuss the temperature and microstructure change rules of specimen during DCT in the following section, two central cross-sections, namely, horizontal (H-H) and vertical (V-V) central planes are taken as the research objects, as presented in Fig. 6. During DCT, the specimen is considered as a mixture phase of austenite and martensite. Initially, the specimen is assumed to have a uniform temperature of 20 °C (room temperature) and be made up of 20% homogeneous retained austenite and 80% homogeneous martensite. The total simulation time is set to 1500 s and the time increment of every step is 0.001 s. The non-linear convective heat transfer boundary condition presented in Fig. 1 is set on the outer

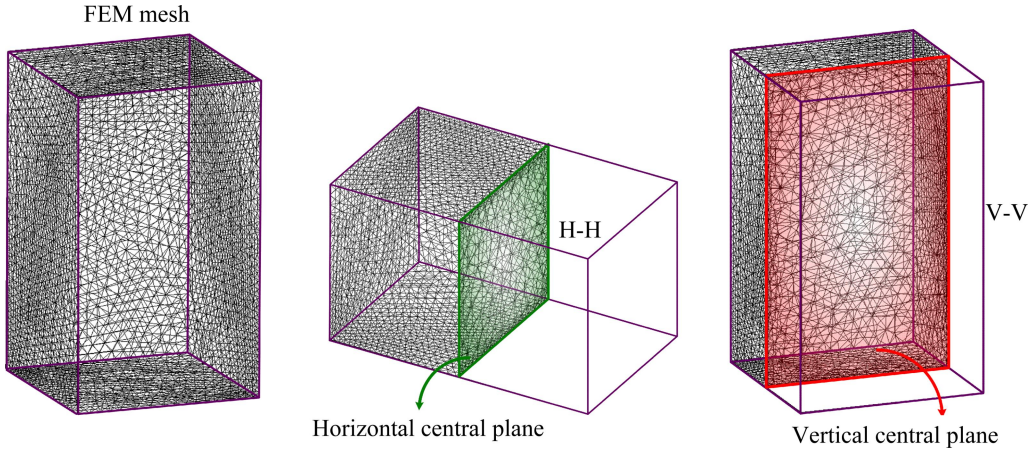

Fig. 6 Three-dimensional FEM models of SDC99 specimen

surface of specimen. The boiling heat transfer coefficient as a function of specimen surface temperature is obtained from the solution of empirical mathematical models, as mentioned in Section 3. Beside the thermal boundary condition, the velocity boundary condition is applied on the vertex of bottom surface, where x, y and z axes are held fixed.

6 Results and discussion

6.1 Temperature distribution during DCT

Figure 7 illustrates the measured and calculated cooling curves and cooling rate curves of SDC99 specimen at different temperature measurement locations. By comparing the simulation results and the experiment results, it can clearly be deduced that, both in terms of the trend and magnitude of temperature and cooling rate, the prediction results show a good agreement with the experimental measurements. Corresponding to the variation characteristics presented in the boiling heat transfer coefficient curve of a specimen immersed in the liquid nitrogen bath, the cooling curve exhibits four distinct boiling heat transfer stages. 1) At the beginning of DCT, the specimen firstly undergoes the stable film boiling stage, as marked with ① in Figs. 7 (a)−(d). The specimen is covered by a continuous film of nitrogen and kept from contacting with the liquid nitrogen. The insulation effect of nitrogen gas reduces the rate of heat transfer and heat transfer coefficient. In this stage, both the measured and calculated cooling curves display an almost linear downward trend. The cooling rate is relatively low around 0.35 °C/s and lasts for longer time. 2) Subsequently, the specimen encounters the transition and nucleate boiling stages, as labeled with ② and ③ in Figs. 7(a)−(d). The point of the maximum boiling heat transfer coefficient is the dividing line between the transition and nucleate boiling. Due to a sudden increase in the boiling heat transfer coefficient, as plotted in Fig. 1, the acute temperature and cooling rate changes occur at this stage and the maximum cooling rate is approximately 1.3 °C/s. Meanwhile, a turning point of temperature from the transition boiling stage to the nucleate boiling stage can be seen on the cooling curve, and the temperature and time corresponding to this point are −93 °C and 370 s, respectively. 3) Finally, the specimen experiences the natural convection stages, as noted with ④ in Figs. 7(a)−(d). In this stage, the temperature of specimen surface is below the boiling point and the heat transfer between the specimen and the liquid nitrogen are performed in a slow and gentle manner. The cooling rate is very little and eventually tends to zero. By comparing and analyzing the measured and calculated cooling curves presented in Figs. 7(a)−(d), it can be found that the cooling behavior at various

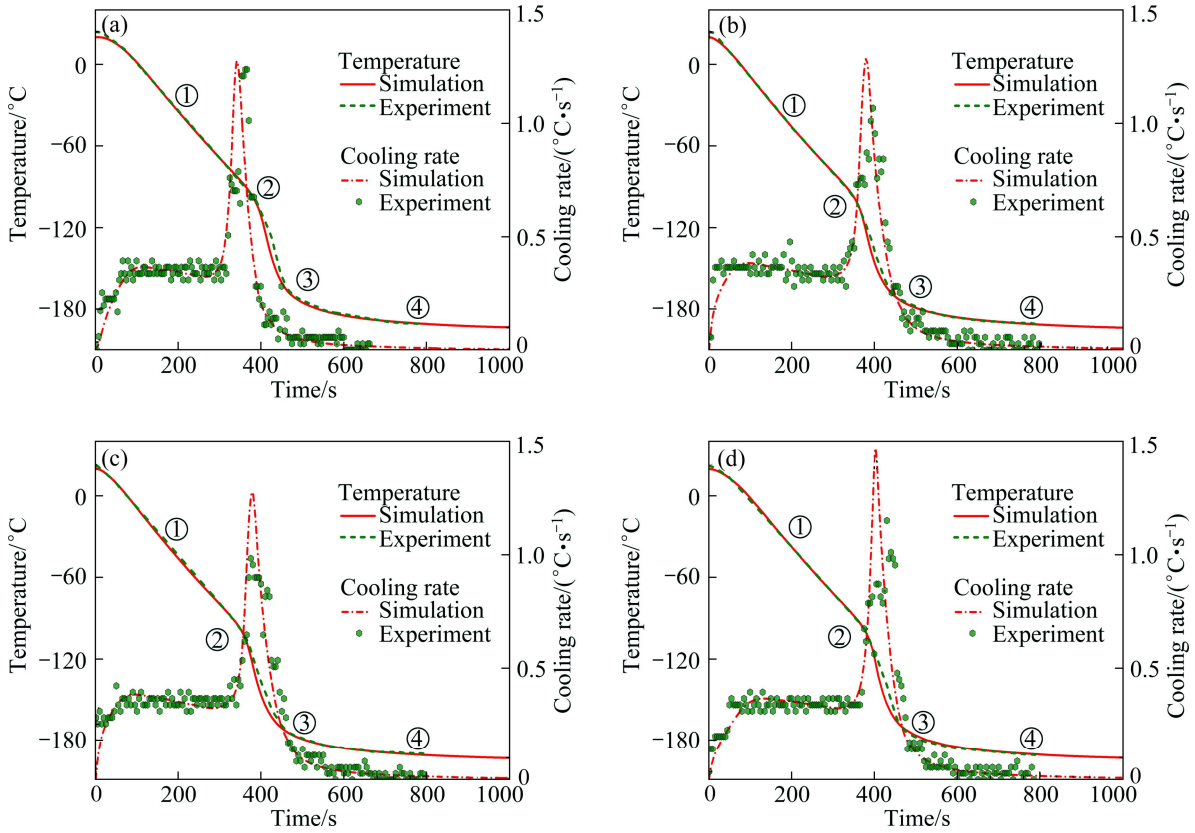

Fig. 7 Measured and calculated cooling curves and cooling rate curves of SDC99 specimen at different temperature measurement locations: (a) Thermoresistor *a*; (b) Thermoresistor *b*; (c) Thermoresistor *c*; (d) Thermoresistor *d*

points of the solidified specimen show the similar trend and the simulation results are consistent with the experimental results. The deviation mainly exists at the transition and nucleate boiling stages, which can be attributed to the transition boiling heat transfer coefficient obtained by a general linearized polynomial interpolation. However, it should be pointed out that these deviations are minor and acceptable.

In order to further explore the temperature field distribution and dynamical evolution rule within the specimen during DCT, such as the cooling rate and the temperature difference between the surface and core of specimen, the horizontal (H-H) and vertical (V-V) central planes of SDC99 specimen are selected to perform a systematic review. Figure 8 gives the cooling rate curves of SDC99 specimen at different positions on the H-H and V-V central planes during DCT. For the H-H central plane, as reported in Fig. 8(a), the cooling rate at the core of specimen reaches its maximum value of 1.27 °C/s when the specimen is immersed in the liquid nitrogen for 410 s, while the maximum cooling rate at the surface of specimen is 4.87 °C/s. The difference of cooling rate between the surface and core of specimen is up to 283%. For the V-V central plane, as plotted in Fig. 8(b), after the specimen is soaked in the liquid nitrogen for 376 s, the cooling rate of specimen surface

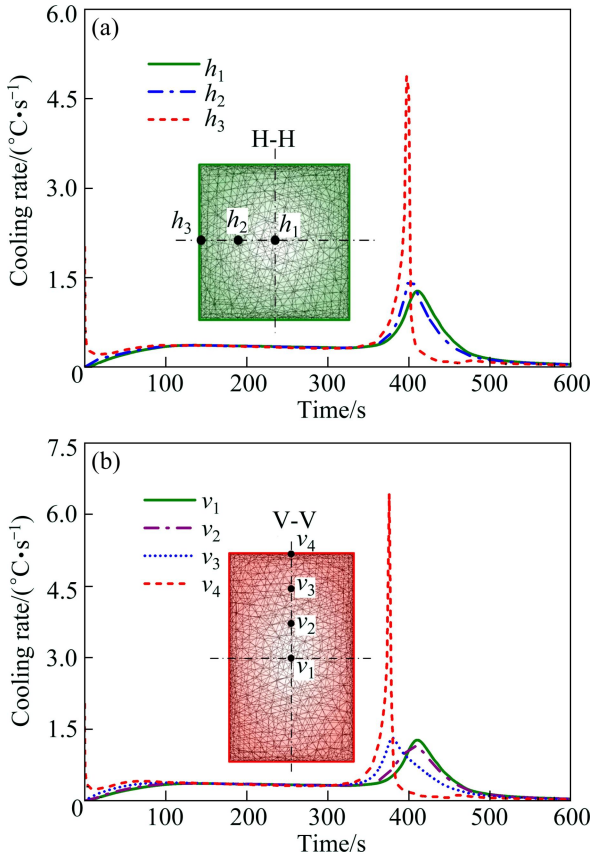

Fig. 8 Cooling rate curves of SDC99 specimen during DCT: (a) Horizontal central plane; (b) Vertical central plane

achieves the maximum value of 4.87 °C/s. The difference of cooling rate between the surface and core of specimen is about 400%. Figure 9 shows the time-dependent temperature difference curves of SDC99 specimen on the H-H and V-V central planes during DCT. For the H-H central plane, the maximum temperature difference between the surface and core of specimen is approximately 49 °C after cooling for 405 s. While, for the V-V central plane, the maximum temperature difference is around 67 °C for the cooling time of 387 s. The above investigation and analysis suggest that the differences in temperature and cooling rate between the surface and core of SDC99 specimen are very significant. However, it is noteworthy that the acute temperature and cooling rate changes during DCT are mainly concentrated on the specimen surface region about 1/3 of the sample thickness, while these changes are performed in a slow and gentle manner at the core region of specimen.

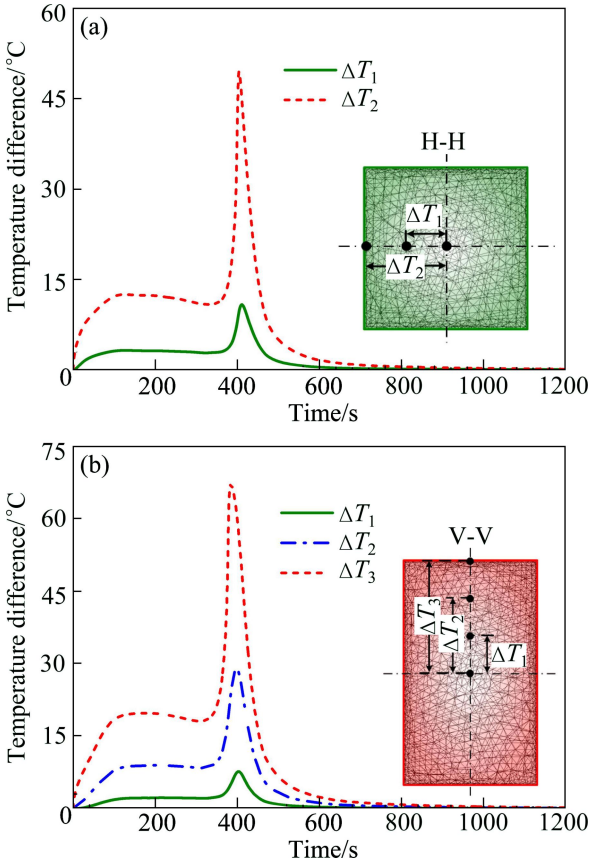

Fig. 9 Temperature difference of SDC99 specimen during DCT: (a) Horizontal central plane; (b) Vertical central plane

6.2 Microstructure distribution during DCT

Numerous investigations concerning the cold work high speed steels have shown that DCT can significantly improve the material properties (especially, the wear resistance, durability and stability) by means of transformation of retained austenite into martensite. The

predicted results of time-dependent phase volume fraction of SDC99 specimen at different positions on the H-H and V-V central planes during DCT are illustrated in Fig. 10. According to Fig. 10, for both the H-H and V-V central planes, the retained austenite in quenched specimen will continue to convert to martensite during DCT. Subjected to DCT, the amount of retained austenite can be significantly decreased and finally its volume fraction is about 2.3%, while the content of martensite increases from 85% to 97.64%. However, it should be emphasized that this phase transformation is incomplete as claimed in Ref. [21].

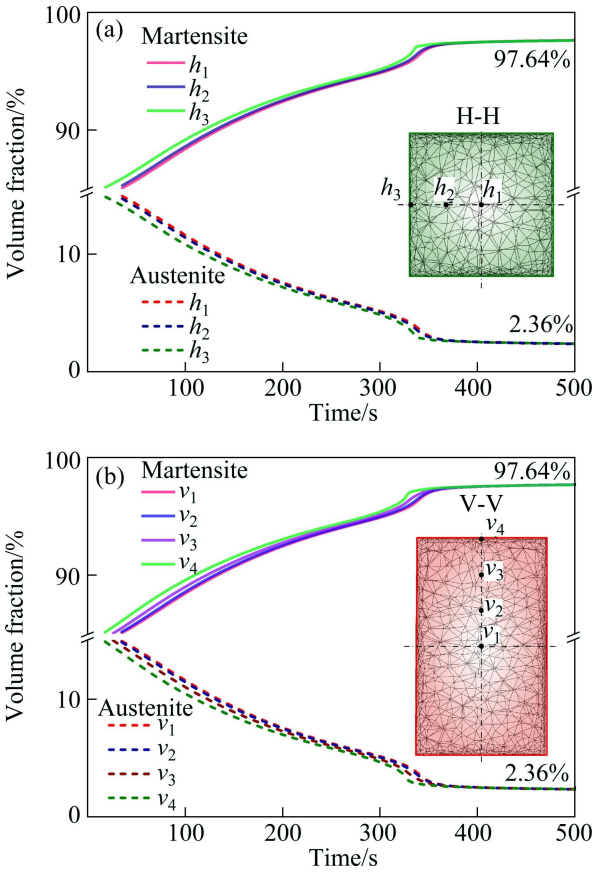

Fig. 10 Phase volume fraction of SDC99 specimen during DCT: (a) Horizontal central plane; (b) Vertical central plane

In order to verify the validity of the above simulation results, the X-ray diffraction technique is used to determine the crystalline structure and measure the contents of retained austenite and martensite of SDC99 specimen. Figure 11 represents the X-ray diffraction pattern and calibration of SDC99 specimen before and after DCT. The peaks corresponding to the retained austenite, martensite and carbides in the XRD pattern are visible. In particular, the peaks (200), (220) and (311) of the retained austenite are considered, as labeled in Fig. 11. It can be seen from this figure that, after DCT, the peaks of the retained austenite exhibit a low intensity value, which validates that the retained austenite transforms into martensite during the DCT process. The experimental results of phase volume fractions of the retained austenite and martensite before and after DCT are 20.3% and 79.7%, 2.8% and 97.2%, respectively. The computational simulation results are coincident well with the experimental data obtained from the X-ray diffraction. In addition, the microstructure of SDC99 specimen before and after DCT has been evaluated by the transmission electron microscopy (TEM), as plotted in Fig. 12. Before DCT, the matrix of SDC99 specimen

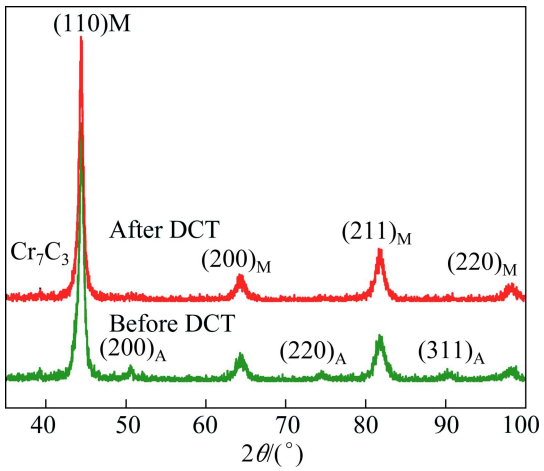

Fig. 11 XRD pattern and calibration of SDC99 specimen before and after DCT

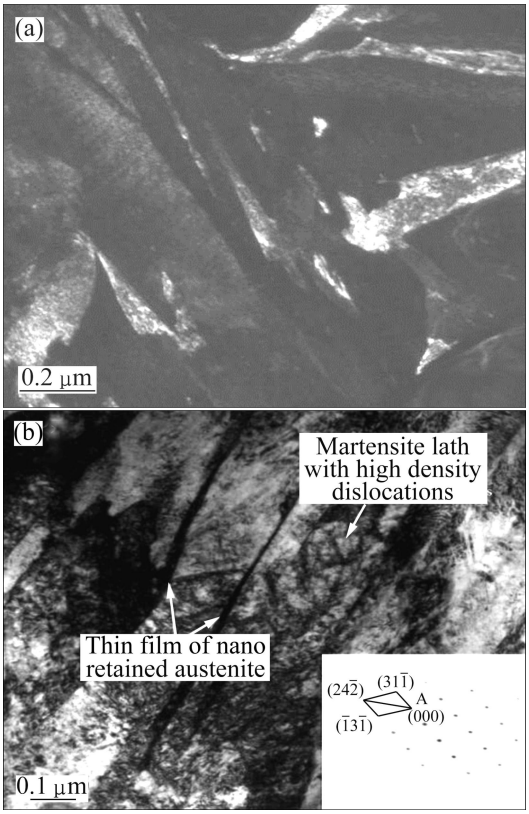

Fig. 12 Morphologies of retained austenite: (a) Before DCT; (b) After DCT

is composed of the lath and plate martensite and thin film retained austenite with a thickness larger than 100 nm. After DCT, the amount of retained austenite can be remarkably reduced. The topography of retained austenite is presented in a nanoscale thin film with a thickness range of 20−60 nm between the martensite laths and stably exists even after prolonged soaking time in liquid nitrogen.

7 Conclusions

1) Combined with the low temperature material properties and the boiling heat transfer coefficient, a numerical model was built to successfully predict the transient temperature distribution during DCT. Moreover, an experimental setup was designed to validate the simulation results. The result demonstrates that the differences in temperature and cooling rate between the surface and core of specimen are very significant. However, it should be emphasized that the acute temperature and cooling rate changes are mainly concentrated on the specimen surface region about 1/3 of the sample thickness, while these changes are performed in a slow and gentle manner at the core region of specimen.

2) Both the experimental and numerical investigations indicate that, subjected to DCT, the retained austenite will continue to transform to martensite until its phase volume fraction is reduced to 2.3%, while the content of martensite will increase from 85% to 97.64%. The numerical results are coincident well with the experimental data obtained from the X-ray diffraction.

3) The coupling numerical model adopted in this study can accurately capture the variation characteristics of temperature and microstructure fields during DCT and provide a theoretical guidance to further evaluate the material properties and make the reasonable DCT procedure.

References

[1] OWAKU S. Cryogenic treatment [J]. Hearing Treatment, 1981, 21(1): 44−48.

[2] COLLINS D N. Deep cryogenic treatment of tool steels: A review [J]. Heat Treatment of Metals, 1995, 23(2): 40−42.

[3] KALSIA N S, SEHGALB R, SHARMA V S. Cryogenic treatment of tool materials: A review [J]. Materials and Manufacturing Processes, 2010, 25(10): 1077−1100.

[4] INOUE T, ARIMOTO K. Development and implementation of CAE system “HEARTS” for heat treatment simulation based on metallo-thermo-mechanics [J]. Journal of Materials Engineering and Performance, 1997, 6(1): 51−60.

[5] LI H P, ZHAO G Q, HE L F. Finite element method based simulation of stress-strain field in the quenching process [J]. Materials Science and Engineering A, 2008, 478(1−2): 276−290.

[6] JIN T, HONG J P. Measurement of boiling heat transfer coefficient in liquid nitrogen bath by inverse heat conduction method [J]. Journal of Zhejiang University: Science A, 2009, 10(5): 691−696.

[7] ZHAO Z D, WANG Y S, WANG Q C, KANG F. Numerical simulation of eliminating residual stress in 7A04 aluminum case by cryogenic treatment [J]. Cryogenics, 2008, 163(3): 30−34.

[8] WANG Q C, KE Y L. Relief of residual stresses in 7075 aluminum alloy by deep cryogenic treatment [J]. Journal of Zhejiang University: Engineering Science, 2003, 37(6): 748−751.

[9] ŞIMŞIR C, GÜR C H. A FEM based framework for simulation of thermal treatments: Application to steel quenching [J]. Computational Materials Science, 2008, 44: 588−600.

[10] BUCHMAYR B, KIRKALDY J S. Modeling of the temperature field, transformation behavior, hardness and mechanical response of low alloy steels during cooling from the austenite region [J]. Journal of Heat Treating, 1990, 8(2): 127−136.

[11] AVRAMI M. Kinetics of phase change. I: General theory [J]. Journal of Chemical Physics, 1939, 7(12): 1103−1112.

[12] INOUE T, FUNATANI K, TOTTEN G E. Process modeling for heat treatment: Current status and future developments [J]. Journal of Shanghai Jiao Tong University, 2000, 5(1): 14−25.

[13] SUGIANTO A, NARAZAKI M, KOGAWARA M, SHIRAYORI A. Numerical simulation and experimental verification of carburizing-quenching process of SCr420H steel helical gear [J]. Journal of Materials processing Technology, 2009, 209(7): 3597−3609.

[14] WESTWATER J W, HWALEK J J, IRIVING M E. Suggested standard method for obtaining boiling curves by quenching [J]. Industrial & Engineering Chemistry Fundamentals, 1986, 25(4): 685−692.

[15] BARRON R F. Crygenic heat transfer [M]. Philadelphia: Taylor & Francis, 1999.

[16] OZISIK M N, ORLANDE H R B. Inverse heat transfer fundamentals and application [M]. New York: Taylor & Francis, 2000.

[17] PANÃO M R O, MOREIRA A L N. Thermo- and fluid dynamics characterization of spray cooling with pulsed sprays [J]. Experimental Thermal and Fluid Science, 2005, 30(2): 79−96.

[18] ROHENSAW J P, HARTENT J P, GANIC M. Handbook of heat transfer [M]. 2rd Ed. New York: McGraw-Hill Book, 1985.

[19] BROMLEY L A. Heat transfer in stable film boiling [J]. Chemical Engineering Progress, 1950, 46(2): 221−227.

[20] SMOLJAN B. Prediction of mechanical properties and microstructure distribution of quenched and tempered steel shaft [J]. Journal of Materials Processing Technology, 2006, 175(1−3): 393−397.

[21] LI S H, DENG L H, WU X C, MIN Y A, WANG H B. Influence of deep cryogenic treatment on microstructure and evaluation by internal friction of a tool steel [J]. Cryogenics, 2010, 50(11−12): 754−758.

深冷处理温度场和组织场的有限元模拟与实验验证

黎军顽[1], 汤磊磊[1], 李绍宏[2], 吴晓春[1]

1. 上海大学 材料科学与工程学院，上海 200072；
2. 昆明理工大学 材料科学与工程学院，昆明 650093

摘　要：结合低温材料参数以及液氮浴沸腾换热系数，基于金属−热−力耦合理论建立深冷处理数值分析模型，再现新型冷作模具钢 Cr8Mo2SiV(SDC99)的深冷处理过程。同时，通过设计深冷处理温度快速测量装置验证模拟结果的准确性。结果表明，深冷处理过程中试样心表温差和冷却速度的差异较大。这种温度和冷却速度的剧烈变化主要集中于从试件表面至心部的 1/3 厚度内。经过深冷处理后，试样内残余奥氏体将继续向马氏体转变，其最终体积分数减小为 2.3%。模拟结果与实验结果非常吻合，这表明采用的数值分析方法能准确地捕捉试件在深冷处理过程中温度场和组织场的变化规律，能为深冷处理工艺的合理制定提供理论依据和借鉴。

关键词：深冷处理; 沸腾换热系数; 有限元; 相变; 冷作模具钢

(Edited by YUAN Sai-qian)